 

*OPTICAL COMPONENTS OF FIBRE-OPTIC COMMUNICATION LINES* https://doi.org/10.1070/QEL17409

# Frequency comb generation in WGM microsphere based generators for telecommunication applications

J. Braunfelds, R. Murnieks, T. Salgals, I. Brice, T. Sharashidze, I. Lyashuk, A. Ostrovskis, S. Spolitis, J. Alnis, J. Porins, V. Bobrovs

*Abstract.* **We review the frequency comb generation process, main microresonator parameters such as free spectral range (FSR) and *Q*-factor, previously used optical frequency comb (OFC) generator parameters and resulting frequency combs, as well as the implementation of OFC for optical data transmission. An optical frequency comb is produced in a setup based on a tapered fibre and a $SiO_2$ microsphere. The generated frequency comb has a frequency spacing of 2 nm or 257 GHz. During the fabrication of a tapered fibre from SMF28, use is made of the transmission signal to control the taper pulling process. The final measured tapered fibre transmission is ~96%. A microsphere whispering gallery-mode resonator (WGMR), exhibiting a *Q*-factor of at least $2 \times 10^7$, is fabricated from an optical fibre with a thicker core than SSMF. Moreover, for future experiments, a frequency comb generator based on a free-space setup consisting of lenses, a prism, and a microsphere is developed, and the *Q*-factor dependence on different distances between the prism and the microsphere is investigated.**

***Keywords:*** *optical frequency comb (OFC), free spectral range (FSR), Q-factor, tapered fibre, $SiO_2$ microsphere resonator.*

## 1. Introduction

Optical frequency combs (OPCs) have revolutionised areas such as optical frequency standards and optical metrology. The resonator-based Kerr frequency combs are capable of replacing expensive arrays of many lasers in passive optical networks (PONs) using wavelength division multiplexing (WDM-PON), which ensures the efficiency of obtaining both spectral and power characteristics.

Since the introduction of OFCs, OFC generators have been used in a variety of applications, including such technologies as optical clocks, RF photonic oscillators with a record spectral purity, applications requiring a precise optical frequency reference, low phase noise microwave systems, coherent optical communications, etc. [1, 2]. It is known that high-*Q* optical resonators enhance third-order nonlinear optical effects by confining the light within a small volume of whispering-gallery-mode resonators (WGMRs), which makes it possible to generate OFCs through the interplay of preferably anomalous group velocity dispersion (GVD) and four-wave mixing (FWM) [3]. As a result, OFC generation was demonstrated by the interaction of a continuous wave (cw) pump laser of a specific frequency with the modes of a nonlinear microresonator [4].

WGMRs are mainly classified by the way of their fabrication. There are spatial resonators, which can be further divided into two microsphere groups: crystalline microdisk resonators produced by polishing $CaF_2$ or $MgF_2$ cylinders and providing a *Q*-factor of $\sim 10^9 - 10^{11}$ [5], and standard telecom fibre-based microspheres produced by melting fibre tip using some heating source, for example, a $CO_2$ laser or a gas flame, providing a *Q*-factor of $\sim 10^6 - 10^9$ (see Table 1). Another common type is integrated microresonators produced from silicon technology compatible material (Si, $Si_3N_4$, etc.) waveguides using lithography techniques, providing a *Q*-factor of $\sim 10^6$ [6] (see Table 2).

Frequency comb generators based on either type of WGMRs demonstrate excellent frequency stability and are significantly simpler (OFC sources consist of a single cw pump laser and a microresonator), and smaller (a resonator diameter ranging from μm to mm) than sources of conventional comb generators [7, 8]. Intrinsic broadband nature of the parametric gain of a WGMR provides a possibility of generating OFCs centred at a wavelength of 1550 nm with a line spacing on the order of tens of hundreds of GHz, spanning over 500 nm (70 THz) [9], or even an octave [10]. It corresponds to optical S, C, L, and U communication bands [11, 12]. Considering also stability and power efficiency [13], OFCs generated in microresonators are an ideal candidate to substitute typically expensive laser array solutions for WDM-PONs [14]. Substitution is possible, because microresonator-based comb sources produce an entire grid of equally spaced optical references needed to sustain a WDM-PON network [2].

Based on the assumption of using Kerr combs in optical communications, several data transmission experiments using integrated WGM resonators have already been demonstrated. For example, the use of $Si_3N_4$ has made it possible to obtain an aggregate data rate of 170.8 Gbit $s^{-1}$ with return-to-zero on-off keying (RZ-OOK) modulation [15], 400 Gbit $s^{-1}$ employing a primary comb [16], 19.7 Tbit $s^{-1}$ over 75 km using a soliton Kerr frequency comb [17], as well as 34.7 Tbit $s^{-1}$ by using advanced modulation format techniques [18]. Also, a data transmission experiment employing a $MgF_2$ crystalline resonator has been performed [19]. However, data transmission based on frequency combs generated in different spatial mic-

**J. Braunfelds, R. Murnieks, T. Sharashidze, A. Ostrovskis, S. Spolitis, J. Porins, V. Bobrovs** Institute of Telecommunications, Riga Technical University, Latvia, Riga, Āzenes street 12, LV;
e-mail: vjaceslavs.bobrovs@rtu.lv;
**T. Salgals, I. Lyashuk** Institute of Telecommunications, Riga Technical University, Latvia, Riga, Āzenes street 12, LV; AFFOC Solutions Ltd., Latvia, Riga, Jelgavas nov., Kalnciems, Jaunības street 2-58, LV-3016; e-mail: Mareks.Parfjonovs@affocs.eu;
**I. Brice, J. Alnis** Institute of Atomic Physics and Spectroscopy, University of Latvia, Latvia, Riga, Jelgavas street 3, LV-1004; e-mail: asi@lu.lv

Received 23 July 2020; revision received 10 August 2020
*Kvantovaya Elektronika* **50** (11) 1043–1049 (2020)
Submitted in English

roresonators, especially fibre-based microsphere resonators, remains to be shown.

The rest of the paper is organised as follows. The fundamentals of frequency comb generation process and main OFC characteristics are described in Section 2. Section 3 focuses on the overall overview of OFC generator implementation and usage in telecommunications. In section 4, further work concepts and experimental results are presented. Finally, conclusions are made showing that frequency combs generated in spatial WGMRs have a potential to substitute the WDM-PON laser array for data transmission.

## 2. Evaluation of the frequency comb generation process

The OFC generation, as first generated in WGMRs [4], is governed by cascaded FWM mediated by the Kerr nonlinearity process in optical materials. Therefore, Kerr frequency combs can be produced in any resonator built from an optical material with Kerr nonlinearity. OFC generation is demonstrated experimentally in $CaF_2$ [8], in $MgF_2$ [7], in $Si_3N_4$ [19], as well as in fibre ring resonators [20]. Numerically, the formation of optical frequency combs in microspheres is simulated based on the Lugiato–Lefever equation, using the split-step Fourier method (SSFM) [21, 22].

When the pump power exceeds a parametric oscillation threshold power within high-$Q$ microresonators, first comb lines emerge at Stokes and anti-Stokes with a spacing of multiples of FSR around pump frequency. Further increase in the pump power initiates cascaded FWM, which produces higher-order sidebands, forming a primary comb. An initially observed line spacing $\Delta$ is reproduced between newly emerged lines due to the conservation of energy in parametric processes. At the next step assisted by degenerate and nondegenerate FWM, secondary lines generate sub-combs with a new resonance spacing $\delta$ from primary lines, which in general differs from $\Delta$. Eventually, sub-combs overlap and form gap-free frequency comb spectrum, and the distance between two sequential comb lines coincide with a resonator free spectral range (FSR) parameter [9, 23]. A gap-free frequency comb possesses one main limiting factor – multiplet lines – but several techniques exist for mitigating the formation of these multiplet lines [13].

A frequency comb generator must have a possibility to adjust the spacing between the comb lines. OFCs usually have a spacing equal to the FSR of the resonators [1]. The WGMR FSR or wavelength range between two resonances can be estimated from the expression:

$$\mathrm{FSR}_{\mathrm{WGM}} = \frac{c}{2\pi a n_0}, \tag{1}$$

where $a$ is the main radius of the resonator and $n_0$ is refractive index at the pump frequency [24].

The comb line spacing can be tuned to be a natural number of FSRs in two ways: by changing coupling conditions [7, 25], or by changing the pump frequency [1, 25], i.e. by detuning the pump laser with respect to the cavity resonance. The pump detuning with respect to the cavity resonance frequency $\Delta = f_{\mathrm{pump}} - f_{\mathrm{cavity}}$ can be positive for a laser with a higher frequency than WGM resonance, called blue-detuned, or negative and therefore smaller, called red-detuned. Blue-detuned excitation is thermally stable at room temperature. Red excitation is thermally unstable, and it is required for soliton formation [26]. Coupling condition modification changes the distance between comb lines and the loaded $Q$-factor (by decreasing resonator loading, the $Q$-factor increases). This, in turn, changes the purity of the frequency comb. The $Q$-factor is a measure of the sharpness (linewidth) of the resonance relative to its centre frequency:

$$Q_{\mathrm{f}} = \frac{\lambda_{\mathrm{res}}}{\mathrm{FWHM}}, \tag{2}$$

where $\lambda_{\mathrm{res}}$ is the resonance wavelength and FWHM is the full width at half maximum characterising the resonance width [27, 28].

The power efficiency of the Kerr comb generation process can be further improved with a proper choice of the microresonator material, weak anomalous dispersion being preferable for OFC generation. The total dispersion profile is affected by the resonator material, shape, and size. Material dispersion for $SiO_2$, $Al_2O_3$, $MgF_2$, $CaF_2$, and $BaF_2$ resonators and total dispersion for different sizes of the $BaF_2$ resonator is calculated and given in [3].

Long-term stabilisation of an optical frequency comb should be ensured to guarantee that the spectral shape and spacing remain stable. Long-term stabilisation can be realised by locking the laser frequency to a cavity resonance. The most popular is the Pound–Drever–Hall (PDH) scheme used in [29, 30]. Other techniques exist, such as self-injection locking, where backscattered light due to the intrinsic Rayleigh scattering is used to lock the laser to a resonance [7, 8].

## 3. Frequency comb generators and their application in telecommunication systems

OFCs find numerous applications in telecommunication systems; for example, Lucas et al. [31] demonstrated a short-reach optical transmission system and reached a data transmission rate of 228 Gb $s^{-1}$ over a 80-cm free-space link. As a second example, OFCs can be used for the generation of microwave signals [32]. Another field where OFCs can be used is fibre-optic transmission systems (FOTS's). Here, the implementation of chip-scale comb sources for data transmission is extensively studied, making it possible to reach data rates up to 50 Tbit $s^{-1}$ of massively parallel WDM data transmission over a considerable distance of 75 km [33]. Also, another potential use of Kerr combs in optical systems is proposed in [34], where multiple Kerr frequency comb (called a slave comb) generation was obtained using different lines from another Kerr comb (called a master comb) located up to 50 km away. However, comb sources based on spatial resonators for data transmission [19] did not get much attention, and so data transmission for OFCs generated in different kinds of spatial resonators, especially fibre-based microspheres, remains to be shown.

Frequency comb generators based on WGM microresonators (see Fig. 1), widely discussed in the literature, typically consist of a cw laser and a polarisation controller (PC). After the controller, the light is amplified with an erbium-doped fibre amplifier (EDFA) and coupled to a nonlinear resonator via prisms, tapered or angle-polished fibres. A bandpass filter (BPF) is used before the microresonator to filter out EDFA noise. Then the light is coupled out from the nonlinear resonator via the same means and is measured with an optical spectrum analyser (OSA) and sent to pin photodiode for analysing frequency comb in the time domain by a digital storage oscilloscope (DSO) or used further in a transmitter (Tx).

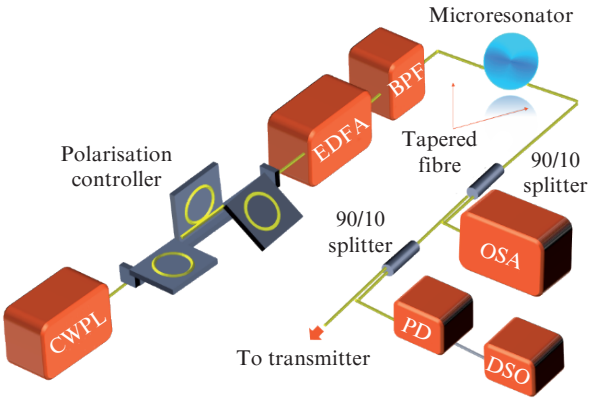


**Figure 1.** Typical WGM comb generator setup (a prism can be used instead of tapered fibres):
(CWPL) continuous-wave pump laser; (EDFA) erbium-doped fibre amplifier; (BPF) bandpass filter; (OSA) optical spectrum analyser; (PD) pin photodiode; (DSO) digital storage oscillator.

Schemes that correspond to this generalised model are, for example, used for pumping resonators in order to generate frequency combs. Parameters for previously performed experiments and microresonators are listed in Tables 1 and 2.

Several data transmission experiments were demonstrated. In one of the first experiments [15], the generation of a Kerr comb was achieved in a silicon nitride resonator. The generated comb was modulated with a RZ-OOK signal up to 42.7 Gb $s^{-1}$. Data transmission is considered error-free if forward error correction (FEC) algorithms are exploited. In a later experiment [19], it was shown that a primary comb generated in a $MgF_2$ crystalline disk resonator provides high-quality carriers that are well-suited for coherent data transmission, because the multiplet line problem is eliminated in this case. A data rate up to 432 Gb $s^{-1}$ is achieved with quadrature phase-shift keying (QPSK) and 16-state quadrature amplitude modulation (16-QAM) formats. A similar data rate of 392 Gb $s^{-1}$ was reached in [16] using a comb generated in $Si_3N_4$ and with the same modulation formats as in [19].

Terabit communications were first demonstrated in [35] with a comb generated in SiN resonators. The stability of the frequency comb is ensured with a feedback signal in the stabilisation loop. The data rate of 1.44 Tbit $s^{-1}$ on 20 channels over 300 km is realised with polarization-division multiplexed quadrature phase-shift keying (PDM-QPSK). Transmission is error-free if FEC with 7% overhead is used. Another terabit rate transmission experiment was performed in [17], where a comb generated in a SiN resonator is used. The data rate of 19.7 Tbit $s^{-1}$ is achieved by transmitting data streams of 224 Gbit $s^{-1}$ on 94 comb lines in the C and L bands. The mod-

**Table 1.** Spatial microresonators and numerical simulations, their parameters and generated frequency combs.

| Parameter | Resonator types | | | |
|---|---|---|---|---|
| | $CaF_2$ [1,24] | $MgF_2$ [7,8,18,35–38] | $SiO_2$ [22,39–44] | Germanosilicate glasses [20,21] |
| | Crystalline | Crystalline | Microsphere\ Microrod\ Microbubble | Microsphere |
| $Q$-factor | $(2.5–6)\times10^9$ | $(1–3)\times10^9$ | $2\times10^7–9.7\times10^8$ | $1\times10^5–1\times10^7$ |
| Radius $a$/mm | 1.275–2.425 | 0.5–5.65 | 0.136–1 | 0.2–0.4 |
| FSR/GHz | 13.8–25 | 5.8–43 | 12.9–1000 | – |
| Pump wavelength $\lambda_{pump}$/nm | 1550–1560 | 1543–1556 | 1549.5–1560 | 1550 |
| Pump power $P_{pump}$/dBm | 14–17 | 3–28.5 | 4.8–24.5 | 20 |
| Comb width/nm | 30–280 | 2–300 | 10–250 | 100–200 |
| Comb spacing/GHz | 13.81–359 | 9.9–248.5 | 32.6–1000 | – |

**Table 2.** Integrated microresonators, their parameters and generated frequency combs.

| Parameter | Resonator types | | | | | |
|---|---|---|---|---|---|---|
| | Silica on a silicon chip [4,50–52] | $Si_3N_4$ [10,11,14,26,33,49] | AlN [47,48] | SiN 16,34] | Hydex glass [46] | $MgF_2$ [45] |
| | Toroidal disk | Ring | Ring | Ring | Four-port microring | Photonic belt |
| $Q$-factor | $(2–2.7)\times10^8$ | $1\times10^5–1.3\times10^6$ | $(5–6)\times10^5$ | $(1–2)\times10^6$ | $1.2\times10^6$ | $4.7\times10^8$ |
| Radius $a$/mm | 0.038–1 | 0.02–0.3 | 0.06 | 0.3 | 0.135 | 1.34 |
| FSR/GHz | 33–850 | 75–403 | 17–370 | 25–95.8 | 200 | 25.78 |
| $\lambda_{pump}$/nm | 1548–1560 | 1541–1561 | 1550–1553.2 | 1548.8–1549.4 | 1544.2–1558.7 | 1561 |
| $P_{pump}$/dBm | 8.8–34 | 21.8–34.8 | 27–27.8 | 29–34.8 | 17.3–18 | 12.8 |
| Comb width/nm | 350–1180 | 200–725 | 200 | – | 100–255 | ~30 |
| Comb spacing/GHz | 33–1100 | 17–403 | 370 | 25–95.8 | 32.7–6400 | – |

ulation format is PDM-16-QAM. All channels, except two, had a bit error rate (BER) below $4.5 \times 10^{-3}$, which is the limit for the 7% overhead FEC. One of the latest experiments regarding WDM data transmission was realised in [18], where the OFC generated in a $Si_3N_4$ microresonator is used for data transmission. Data rates of around 30 Tbit $s^{-1}$ were achieved by encoding data on approximately 100 GHz spaced 94 comb lines using 16-QAM.

## 4. WCOMB generation based on WGM microsphere resonators

The performed experiments, results, and methods described in the following section are promising for telecommunication applications, for example, in terms of a multi-wavelength light source for optical transmission systems. Below we discuss two whispering gallery mode resonator-based optical frequency comb (WCOMB) generation methods. The first method (see Fig. 2) is based on a $SiO_2$ microsphere WGMR and a tapered fibre, while the second method (see Fig. 4) is based on a free-space setup consisting of lenses, a prism, and a microsphere WGMR. The most crucial element in both approaches is the high-$Q$ WGMR microsphere. Such microsphere WGMRs exhibit a $Q$-factor of at least $2 \times 10^7$, which is defined by a smooth surface, low intrinsic losses, and by outcoupling [27, 53]. During our research, we established that the optimal microsphere WGMR diameter is 270 μm.

### 4.1. Experimental setups for WCOMB generation

For the realisation of the first-scenario setup (see in Fig. 2.) for WCOMB generation, we fabricated a $SiO_2$ microsphere and a tapered fibre. According to previous research [54], a hydrogen ($H_2$) flame is used to melt the $SiO_2$ optical fibre tip [with a core several times thicker than that of the standard single-mode optical fibre (SSMF)] for the fabrication of a microsphere WGMR. Such fibre is produced in Latvia by Light Guide Optics. Before tapered fibre fabrication, it is necessary to remove optical fibre coating and jacket, which can be done with mechanical or chemical methods. For this scenario, the mechanical method is employed, because it is not entirely clear what materials and mixtures are used for optical fibre coating and jacket layers. Typically, the mechanical method is realised as follows: the fibre is cut in half, and the coating and jacket layers are removed. After that, cleaned fibre ends are spliced together with fusion splicer equipment. For optical fusion splicing, we used a Sumitomo Fusion Splicer - T 71C is used with auto parameters for ITU-T G. 652 fibre. The fusion splicing spot is protected by a splice protection sleeve.

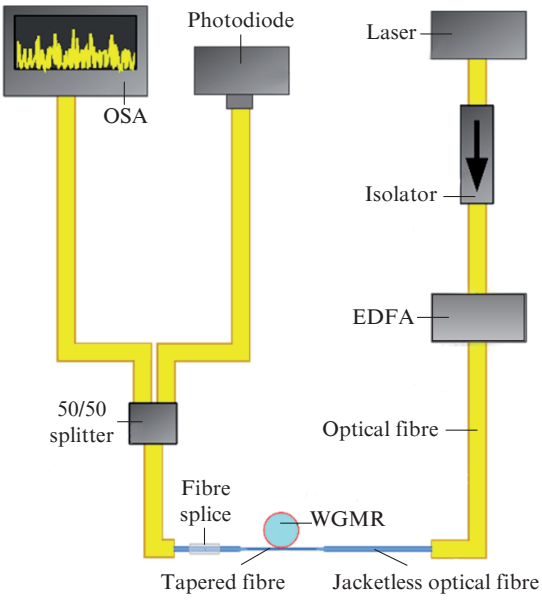


**Figure 2.** WCOMB generation setup based on a $SiO_2$ microsphere WGMR and tapered fibre.

When fibre is spliced, tapering is performed by using a $H_2$ flame. A single-mode optical fibre (SMF28) is tapered with a constant speed of 80 μm $s^{-1}$, and the tapering length is 21–23 mm. The monitored transmission signal during taper pulling is shown in Fig. 3. This signal allows us to behold when the fibre cladding and core melt and the single-mode fibre becomes multi-mode. As the fibre is stretched more, it eventually becomes single mode again (in 280–285 s, see Fig. 3). The duration of the tapering process is 290 s. Before optical fibre tapering, the signal amplitude is 3.92 V, but after it is 3.75 V and the resulting final transmission is equal to ~96%.

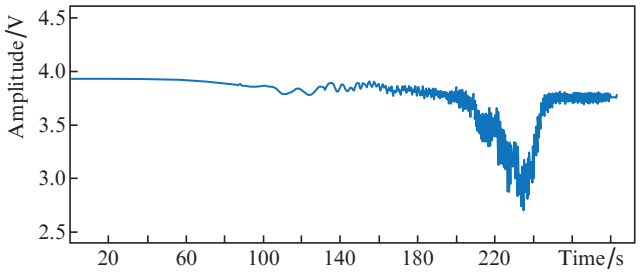


**Figure 3.** Transmission monitoring during taper pulling.

In the transmission part of the setup, a 40-mW single-mode optical laser with a centre wavelength of 1550 nm (Thorlabs SFL1550S) is used in the scanning regime to generate an optical signal. At pump laser power level necessary for comb generation, the microsphere heats up, and this thermal effect distorts and shifts the resonance away from the excitation line. To generate a frequency comb, the laser frequency must come quicker into resonance with the WGM line than the resonator heating time [39]. The Kerr effect responsible for comb generation is instantaneous. To generate a Kerr comb, we swept laser current by a triangular ramp at a repetition rate of about 1 kHz with a laser frequency offset of 2 GHz.

The laser output is connected to an optical isolator for laser protection from reflected signals. The optical isolator output is connected to the EDFA to amplify the optical signal power. The EDFA output power is fixed at 20 dBm, and its output is connected to SMF28 single-mode optical fibre (900 μm jacket), used to fabricate the tapered fibre.

In the receiving part, an Y-type 50/50 optical power splitter is used to ensure parallel monitoring. One of the monitoring ports is connected to a high resolution (0.01 nm) OSA, but the second port is connected to an InGaAs photodetector for a wavelength band of 800–1800 nm. The photodetector is connected to a signal oscilloscope for signal resonance monitoring. For WCOMB generation, it is essential to control the distance between tapered fibre and a microsphere WGMR

(see Section 4.2). Air flows that appear around thin tapered fibre and a microsphere dislocate these two elements. The distance between them changes, which in turn changes the coupled pump power, causing frequency comb spectrum fluctuations. Therefore, the tapered optical fibre needs to be stretched and integrated into a box for limiting air flows. Integration in a box also helps to protect taper fibre and a microsphere WGMR from dust, which change the $Q$-factor of the microsphere because of the light losses due to the dust particles.

The second-scenario setup (Fig. 4) for WCOMB generation is based on the free-space setup consisting of lenses, a prism, and a WGMR. The setup can be easily connected and integrated into a box. In the transmission part of the setup, the same 40-mW single-mode optical laser diode is used as in the first scenario. The optical laser (the wavelength is fixed at 1550 nm) is used in the scanning regime. The optical coupling prism is one of the main components of the setup. An optical lens is used to focus the beam on the optical prism's surface, where total internal reflection occurs. To couple the optical signal into the microsphere WGMR resonator, an $XYZ$ translation stage is used as the resonator has to be aligned with the total internal reflection point. A piezoelectric motor is used to control the translation stage to achieve critical coupling. In the receiving part of the setup, an InGaAs photodetector (a wavelength band of 800–1800 nm) is used for signal resonance monitoring.

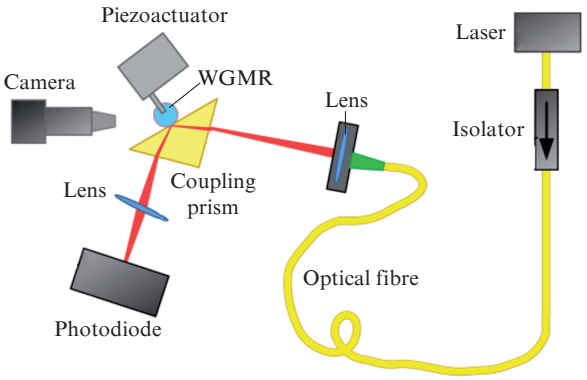


**Figure 4.** WCOMB generation setup based on free-space setup consisting of lenses, a prism, and a microsphere WGMR.

### 4.2. Results and discussion

The set goals were reached and we successfully generated the first optical frequency comb in our setup based on tapered fibres and a $SiO_2$ microsphere WGMR. The first optical frequency comb generated in our setup is shown in Fig. 5. As we can see from the optical spectrum, the comb spacing is 2 nm or 257 GHz comparable to those shown in [11, 14, 18, 22, 24]. The OSA spectrum was recorded during the laser frequency sweep in the experiment presented here. In the future, we will implement feedback locking of the laser and WGM resonance to achieve a stationary comb spectrum [39]. The comb spectrum displays the absence of some lines. This absence could be explained by laser sweeping but also by mode crossing effect as the microsphere resonator has a rich mode spectrum. When two spatial modes come into resonance at the same wavelength, the comb line's intensity drops due to power transfer to another mode family [55, 56].

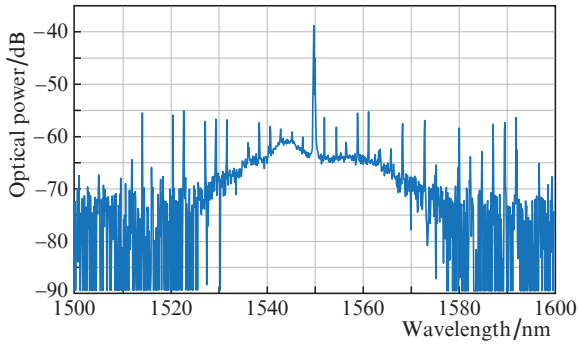


**Figure 5.** Optical spectrum of the first OFC generated in the setup shown in Fig. 2.

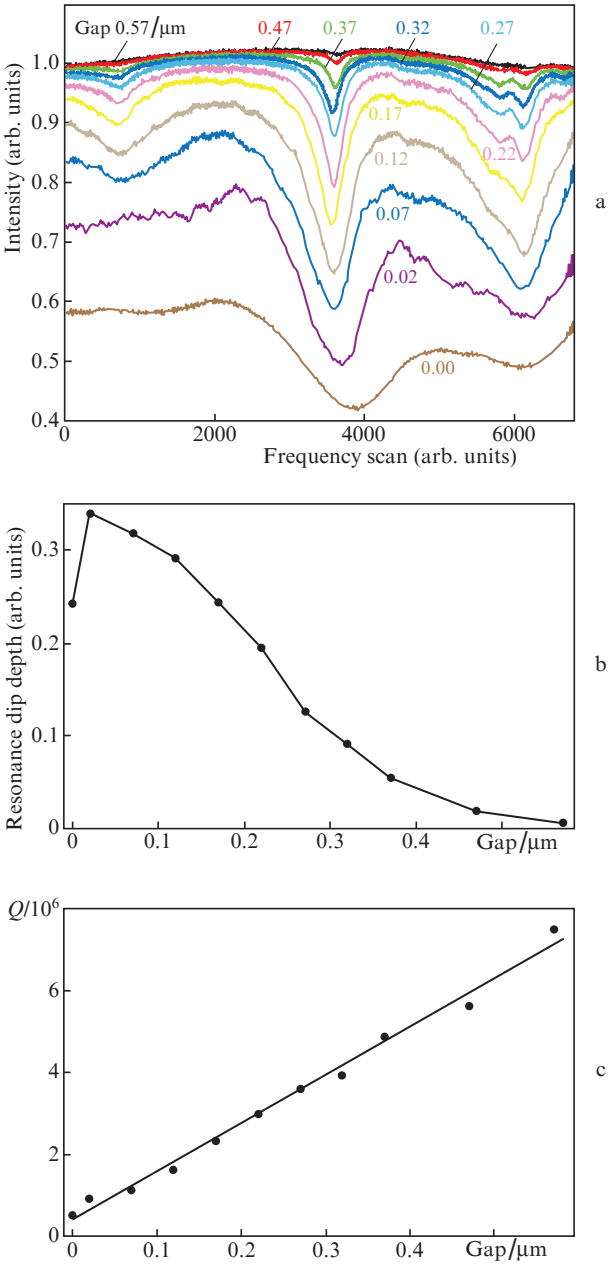


**Figure 6.** (Colour online) Coupling conditions as functions of the gap between the prism and the microsphere resonator (second scenario) the gap is slowly narrowed: (a) transmission spectra for the WGM resonances , (b) resonance dip depth changes, and (c) $Q$-factor.

As mentioned in Section 2, the coupling condition adjustment changes the $Q$-factor of the resonator. An adjustment here means changing the distance between microsphere and prism, and therefore changing resonator loading. The $Q$-factor defines how long the pump light is confined within a resonator, and by minimising coupling losses (increasing distance), it is possible to increase the $Q$-factor [2]. From equation (2), we can see that narrower resonance FWHM ensures a larger $Q$-factor. Thus, we can say that by increasing the distance between prism and microsphere, FWHM becomes narrower, as seen in Fig. 6a. The increase in the $Q$-factor is demonstrated in Fig. 6c. The $Q$-factor was estimated using the following technique: First, the frequency scale was recalibrated from arbitrary units to MHz using a signal electro-optic modulator (EOM). The modulation frequency of 100 MHz provided sidebands on both sides of the resonance. The WGM resonance peak was fitted using a Lorentzian function to calculate the FWHM. The $Q$-factor was calculated with the equation: $Q = f/\Delta f$, where $f$ is the frequency of the light and $\Delta f$ is the full width at half maximum of the resonance.

Resonator loading can be described with three distinct coupling regimes: under-coupling, over-coupling, and critical coupling [57]. In the under-coupling regime, the prism is far away (0.57 μm) from the microsphere. The coupled pump power is too small (despite low coupling losses) to overcome intrinsic losses due to the absorption, which is seen by the resonance intensity, for example, in Fig. 6a. When the gap is 0.47 μm, the resonance dip depth (in arb. units) is $\sim 0.025$ (see Fig. 6b), but the $Q$-factor is $\sim 6 \times 10^6$ (see Fig. 6c). In the over-coupling regime, the light power within the resonator and the coupling losses are high, but the $Q$-factor is small. For example, when in the case of a zero gap, the $Q$-factor is $\sim 5 \times 10^5$, but resonance dip depth is $\sim 0.25$. The preferable regime is critical coupling when the trade-off between the coupled pump power and coupling losses is in balance. By taking into account the mentioned facts, we conclude that the optimal gap between prism and microsphere is 0.12 or 0.17 μm.

## 5. Conclusions

We have reviewed previously performed experiments of frequency comb generation and its applications for telecommunications. A discussion of the applications of frequency combs in different fields, such as the usage of frequency combs generated in near-infrared and mid-infrared regions, is left beyond the scope of the paper. The generalised frequency comb generator model is constructed based on already used generators utlising different kinds of microresonators. The main frequency comb generator parameters and characteristics used in previous studies are discussed and summarised in Tables 1 and 2. We have also investigated the frequency comb generation in the setup based on a tapered fibre and a microsphere WGMR. The generated frequency comb has a frequency spacing of 2 nm or 257 GHz. For the fabrication of the tapered fibre, we designed a fibre pulling installation, which ensures the resulting final transmission of $\sim 96\%$. The tapered fibre is fabricated from SMF28 fibre. To control the taper pulling process, we monitored the transmission signal. A microsphere WGMR, exhibiting a $Q$-factor of at least $2 \times 10^7$ and optimal 270-μm diameter, is fabricated from an optical fibre (produced in Latvia) with a thicker core than that of a standard single-mode fibre. For future experiments, a frequency comb generator based on the free-space optics setup is fabricated, and the importance of the gap between the prism and the microsphere is demonstrated. We found out that the preferable gap length is 0.12 or 0.17 μm. We will also continue to work on the improvements of microresonator quality.

***Acknowledgements.*** This work was supported by the European Regional Development Fund (Project No. 1.1.1.1/18/A/155 "Development of an optical frequency comb generator based on a whispering gallery mode microresonator and its applications in telecommunications").

## References

1. Savchenkov A.A., Matsko A.B., Ilchenko V.S., Solomatine I., Seidel D., Maleki L. *Phys. Rev. Lett.*, **101**, 093902 (2008).
2. Savchenkov A.A., Matsko A.B., Maleki L. *Nanophotonics*, **5**, 363 (2016).
3. Lin G., Diallo S., Chembo Y.K. *Proc. 17th Intern. Conf. on Transparent Optical Networks (ICTON) 2015* (Budapest, 2015) p. 1.
4. Del'Haye P., Schliesser A., Arcizet O., Wilken T., Holzwarth R., Kippenberg T.J. *Nature*, **450**, 1214 (2007).
5. Liopis O., Merrer P.H., Bouchier A., Saleh K., Cibiel G. *Proc. SPIE*, **7579**, 75791B (2010).
6. Pasquazi A., Peccianti M., Razzari L., Moss D.J., Coen S., Erkintalo M., Chembo Y.K., Hansson T., Wabnitz S., Del'Haye P., Xue X., Weiner A.M., Morandotti R. *Phys. Rep.*, **729**, 1 (2018).
7. Liang W., Savchenkov A.A., Matsko A.B., Ilchenko V.S., Seidel D., Maleki L. *Opt. Lett.*, **36**, 2290 (2011).
8. Liang W., Matsko A.B., Savchenkov A.A., Ilchenko V.S., Seidel D., Maleki L. DOI: 10.1109/fcs.2011.5977756.
9. Pfeifle J. *Karlsruhe Series in Photonics & Communication*, **20** (2017).
10. Levy J.S., Gondarenko A., Foster M.A., Turner-Foster A.C., Gaeta A.L., Lipson M. *Nat. Photonics*, **4**, 37 (2010).
11. Foster M.A., Levy J.S., Kuzucu O., Saha K., Lipson M., Gaeta A.L. *Opt. Express*, **19**, 14233 (2011).
12. Jazayerifar M., Jamshidi K. *Proc. 2016 IEEE Photonics Soc. Summer Topical Meeting Series (SUM)* (Newport Beach, 2016) p. 84.
13. Kurbatska I., Bobrovs V., Alsevska A., Lyashuk I., Gegere L. *Progress in Electromagnetics Research Symposium* (St. Petersburg, 2017) pp 1771–1777. DOI: 10.1109/PIERS.2017.8262037.
14. Pfeifle J., Weimann C., Bach F., Riemensberger J., Hartinger K., Hillerkuss D., Jordan M., Holtzwarth R., Kippenberg T.J., Leuthold J., Freude W., Koos C. *Proc. 2012 Optical Fiber Communication Conf.* (Los Angeles, 2012) p. 3.
15. Pfeifle J., Lauermann M., Wegner D., Brasch V., Herr T., Hartinger K., Li J., Hillerkuss D., Schmogrow R., Holtzwarth R., Freude W., Leuthold J., Kippenberg T.J., Koos C. *Nat. Photonics*, **8**, 375 (2014).
16. Pfeifle J., Kordts A., Marin P., Karpov M., Pfeiffer M.H., Brasch V., Rosenberger R., Kemal J., Wolf S., Freude W., Kippenberg T.J., Koos C. *Proc. Conf. on Lasers and Electro-Optics (CLEO) 2015* (San Jose, 2015) p. 2.
17. Marin-Palomo P., Kemal J.N., Karpov M., Kordts A., Pfeifle J., Pfeiffer M.H., Trocha P., Wolf S., Brasch V., Anderson M.H., Rosenberger R., Vijayan K., Freude W., Kippenberg T.J., Koos C. *Nature*, **546**, 274 (2017).
18. Pfeifle J., Coillet A., Henriet R., Saleh K., Schindler P., Weimann C., Freude W., Balakireva I.V., Larger L., Koos C., Chembo Y.K. *Phys. Rev. Lett.*, **114**, 093902 (2015).
19. Avino S., Giorgini A., Malara P., Gagliardi G., Natale P.D. *Opt. Express*, **21**, 13785 (2013).
20. Anashkina E.A., Sorokin A.A., Marisova M.P., Andrianov A.V. *Quantum Electron.*, **49**, 371 (2019) [*Kvantovaya Elektron.*, **49**, 371 (2019)].
21. Sorokin A.A., Marisova M.P., Andrianov A.V., Anashkina E.A. *Proc. Intern. Conf. on Information Science and Communications Technologies (ICISCT)* (Tashkent, Uzbekistan, 2019).
22. Song Z., Lei S., Linhao R., Yanjing Z., Bo J., Bowen X., Xinliang Z. *Nanophotonics*, **8**, 2321 (2019).
23. Coillet A., Balakireva I., Henriet R., Saleh K., Larger L., Dudley J.M., Menyuk C.R., Chembo Y.K. *IEEE Photon. J.*, **5**, 6100409 (2013).

24. Grudinin I.S., Yu N., Maleki L. *Opt. Lett.*, **34**, 878 (2009).
25. Kippenber T.J., Gaeta A.L., Lipson M., Gorodetsky M.L. *Science*, **361**, 6402 (2018).
26. Herr T., Hartinger K., Riemensberger J., Wang C.Y., Gavartin E., Holzwarth R., Gorodetsky M.L., Kippenberg T.J. *Nat. Photonics*, **6**, 480 (2012).
27. Bogaerts W., De Heyn P., Vaerenbergh T.V., De Vos K., Selvaraja S.K., Claes T., Dumon P., Bienstman P., Van Thorhout D., Baets R. *Laser Photonics Rev.*, **6**, 47 (2012).
28. Loh W., Yegnanarayanan S., O'Donnell F., Juodawlkis P.W. *Optica*, **6**, 152 (2019).
29. Liang W., Savchenkov A.A., Ilchenko V.S., Eliyahu D., Matsko A.B., Maleki L. *IEEE Photon. J.*, **9**, 5502411 (2017).
30. Zhang J., Li F., Li J., Li Z. *Proc. 16th Intern. Conf. on Optical Communications and Networks (ICOCN) 2017* (Wuzhen, 2017) p. 3.
31. Lucas E., Jost J.D., Kippenberg T.J., Beha K., Lezius M., Holzwarth R. *Proc. Joint Conf. EFTF/IFCS* (Besancon, 2017) pp 530 – 533.
32. Marin P., Pfeifle J., Karpov M., Trocha P., Rosenberger R., Vijayan K., Wolf S., Kemal J., Kordts A., Pfeiffer M., Brasch V., Freude W., Kippenberg T.J., Koos C. *Proc. Conf. on Lasers and Electro-Optics (CLEO) 2016* (San Jose, USA, 2016) p. 2.
33. Liao P., Bao C., Almaiman A., Kordts A., Karpov M., Pfeif- fer M.H.P., Zhang L., Alishahi F., Cao Y., Zou K., Fallahpour A., Willner A.N., Tur M., Kippenberg T.J., Willner A.E. *J. Light. Wave Technol.*, **37**, 579 (2019).
34. Pfeifle J., Yu Y., Schindler P.C., Brasch V., Herr T., Weimann C., Hartinger K., Holzwarth R., Freude W., Kippenberg T.J., Koos C. *Proc. 2014 Optical Fiber Communication Conf.* (San Francisco, 2014) p. 3.
35. Herr T., Wang C.Y., Del'Haye P., Schliesser A., Hartinger K.K., Holtzwarth R., Kippenberg T.J. *Proc. Conf. on Lasers and Electro-Optics (CLEO) 2011* (Baltimore, 2011) paper QTuF1.
36. Herr T., Hartinger K., Riemensberger J., Wang C.Y., Gavartin E., Holzwarth R., Gorodetsky M.L., Kippenberg T.J. *Nat. Photonics*, **6**, 480 (2012).
37. Liang W., Eliyahu D., Ilchenko V.S., Savchenkov A.A., Matsko A.B., Seidel D., Maleki L. *Nat. Commun.*, **6**, 7975 (2015).
38. Pavlov N.G., Lihachev G., Koptyaev S., Voloshin A.S., Ostapchenko A.D., Gorodnitskiy A.S., Gorodetsky M.L. *Proc. 19th Intern. Conf. on Transparent Optical Networks (ICTON) 2017* (Girona, Spain, 2017) p. 3.
39. Agha I.H., Okawachi Y., Gaeta A.L. *Opt. Express*, **17**, 16209 (2009).
40. Ming L., Xiang W., Liying L., Lei X. *Opt. Express*, **21**, 16908 (2013).
41. Papp S.B., Del'Haye P., Diddams S.A. *Phys. Rev. X*, **3**, 31003 (2013).
42. Webb K.E., Jang J.K., Anthony J., Coen S., Erkintalo M., Murdoch S.G. *Opt. Lett.*, **41**, 277 (2016).
43. Webb K.E., Erkintalo M., Coen S., Murdoch S.G. *Opt. Lett.*, **41**, 4613 (2016).
44. Kubota A., Suzuki R., Fujii S., Tanabe T. *Proc. CLEO/Europe-EQEC* (Munich, 2017). DOI 10.1109/CLEOE-EQEC.2017.8087288.
45. Grudinin I.S., Huet V., Yu N., Matsko A.B., Gorodetsky M.L., Maleki L. *Optica*, **4**, 434 (2017).
46. Razzari L., Duchesne D., Ferreram M., Morandottim R., Chum S., Little B.E., Moss D.J. *Nature Photon.*, **4**, 41 (2010).
47. Jung H., Xiong C., Fong K.Y., Zhang X., Tang H.X. *Opt. Lett.*, **38**, 2810 (2013).
48. Hojoong J., King F.Y., Chi X., Hong T.X. *Opt. Lett.*, **39**, 84 (2014).
49. Levy S., Saha K., Okawachi Y., Foster M.A., Gaeta A.L., Lipson M. *IEEE Photon. Technol. Lett.*, **24**, 1375 (2012).
50. Del'Haye P., Schliesser A., Arcizet O., Wilken T., Holzwarth R., Kippenberg T.J. *Nature*, **450**, 1214 (2007).
51. Del'Haye P., Herr T., Gavartin E., Holzwarth R., Kippenberg T.J. *Phys. Rev. Lett.*, **107**, 063901 (2009).
52. Li J., Lee H., Chen T., Vahala K.J. *Phys. Rev. Lett.*, **109**, 233901 (2012).
53. Fulop A. *Fiber-Optic Communications with Microresonator Frequency Combs* (Gothenburg: Chalmers University of Technology, 2018).
54. Brice I., Grundsteins K., Atvars A., Alnis J., Viter R., Ramanavicius A. *Sensors and Actuators B: Chem.*, **318**, 128004 (2020).
55. Fujii S., Tanabe T. *Nanophotonics*, **9** (5), 2019 (2020).
56. Savchenkov A.A., Matsko A.B., Liang W., Ilchenko V.S., Seidel D., Maleki L. *Opt. Express*, **20**, 27290 (2012).
57. Demirtzioglou I., Lacava C., Bottrill K.R.H., Thomson D.J., Reed G.T., Richardson D.J, Petropoulos P. *Opt. Express*, **26**, 790 (2018).